What we (possibly) know about the 3-D structure of crust and mantle beneath the Alpine chain

Anne Paul

2

What we (possibly) know about the 3-D structure of crust and mantle beneath the Alpine chain

Anne Paul[1]

[1] *Univ. Grenoble Alpes, Univ. Savoie Mont Blanc, CNRS, IRD, UGE, ISTerre, 38000 Grenoble*

Introduction

In 1993, E. Kissling published a seminal paper that presented a review of available geophysical data on the structure of the crust and upper mantle under the Alps and an assessment of the uncertainties associated with these data (Kissling 1993). The abstract of this publication began with the following sentence: « In the last five decades, the deep structure of the Alps has been probed by every geophysical method applicable, and the resulting amount of data is unmatched for any other orogen ». Indeed, the publication came after a decade of major deep reflection or refraction seismic surveys in the central Alps (European Geotraverse: Blundell et al. 1992; Swiss NFP20 program: Frei et al. 1990) and in the western Alps (ECORS-CROP: Nicolas et al. 1990). These large seismic data acquisition

[Book title],
coordinated by [Book coordinator].

programs (complemented with a gravimetric survey for ECORS-CROP: Bayer et al. 1989) provided E. Kissling with the main argument that the available data set on the deep structure of the Alps was quite unique for a mountain range. These data were all related to crustal structure, internal structure by vertical seismic reflection, and Moho depth for wide-angle seismic and refraction.

In the early 1990s, the structure of the upper mantle beneath the Alps began to be studied by teleseismic tomography, which is traveltime tomography of waves emitted by distant earthquakes (epicentral distances > 20°) and recorded by permanent seismic stations (Babuška et al. 1990; Cattaneo and Eva, 1990; Spakman 1990, 1991). Critical examination of these results by Kissling (1993) led him to conclude that a slab of European lithosphere is dipping southwards in the mantle beneath the southern central Alps and the Po basin. A few years later, the development of permanent seismological networks and the collection and distribution by ISC (International Seismological Centre, http://www.isc.ac.uk) of a global seismological bulletin with hypocenter locations and arrival time picks have allowed increasingly accurate arrival time tomography, such as that of Piromallo and Morelli (2003) for the Alpine-Mediterranean area. Their P-wave velocity anomaly maps between 100 and 250 km depth clearly show the fast anomaly associated with the subduction of the European slab in the mantle of the western and central Alps. The anomaly is much less clear under the eastern Alps. The mantle transition zone (410-660 km depth) is characterized by fast P-wave velocities over most of the Alpine-Mediterranean region. Piromallo and Faccenna (2004) interpreted this result using geological data on Alpine convergence and kinematic reconstructions. They proposed that most of the fast-velocity anomalies detected in the mantle transition zone correspond to slab fragments detached from the Alpine subduction by an event occurring around 30-35 Ma.

The teleseismic tomography of the Alpine mantle by Lippitsch et al. (2003) showed for the first time a high-velocity anomaly with a steep northeast dip under the eastern Alps. On the basis of this dip, they interpreted this anomaly as evidence of subduction of the continental lithosphere of the Adria microplate under Europe. Lippitsch et al. (2003) also confirmed the presence of south-eastward dipping slabs under the western and central Alps, evidence of subduction of the European plate under Adria. This tomography was the first to use all the seismological data from the permanent networks available in the region, even though not all of them were open. They carefully picked all arrival times in a homogeneous way, and they took into account lateral variations in crustal structure by applying crustal corrections calculated in a 3-D model. Thanks to the quality and accuracy of the work carried out by Lippitsch et al. (2003), from the preparation to the analysis and then the

inversion of the P-wave arrival time data set, this publication has become an important reference on the structure of the Alpine uppermost mantle.

Over the past decade or so, seismic imaging of the lithosphere has benefited from a dual revolution in data and methods. Advances in seismological instrumentation have led to the development of broadband seismometers which today equip most of the permanent seismological networks installed in the Alps. Instruments of similar quality can also be deployed in large numbers on temporary experiments lasting from a few months to a few years to improve the spatial coverage of permanent networks (e.g. AlpArray, http://www.alparray.ethz.ch/; AlpArray Seismic Network 2015; Hetényi et al. 2018a). Last but not least, most of the high-quality data provided by these permanent and temporary stations are now open and accessible to all thanks to the European federation of seismological datacenters EIDA (European Integrated Data Archive, http://www.orfeus-eu.org/data/eida/). This data revolution now makes large volumes of high-quality seismological data readily available.

The other revolution concerns tomography methods. It is of course related to the development of the performance of computers, but it remains inseparable from the data revolution: the most modern tomography is blind without a large amount of high-quality data. Much more than just arrival times, we now know how to use the entire seismic record in all its complexity in terms of amplitude and phase to probe the fine structure of the subsurface. This is achieved by full waveform inversion (FWI) that theoretically gives access to all the elastic parameters, P-wave velocity, S-wave velocity and density, as well as other physical parameters such as anisotropy or attenuation (e.g. Tape et al. 2009). Finally, we even know how to probe the subsurface without illumination by an earthquake or a man-made source, using ambient seismic noise. Campillo and Paul (2003) and Shapiro and Campillo (2004) have shown that correlating long time series of noise records at two seismic stations results in the same signal as if a seismic source were placed at one of the two stations and the waves recorded at the other station. Each seismic station thus becomes a wave source for all the others. This method has great potential for seismic imaging in regions with low to moderate seismicity, which is the case for a large part of the Alps.

Since the review by Kissling (1993) and key publications by Lippitsch et al. (2003) and Piromallo and Morelli (2003) on the structure of the Alpine upper mantle, several temporary passive seismic experiments (as opposed to active seismic reflection or refraction profiling) have been carried out in the Alps, either along profiles transverse to the belt or in deployments of sensor arrays such as AlpArray (Figure 2.1). Seismic tomography work was also carried out using data from

permanent networks. I will review this work in the following parts of this chapter, starting with imaging of the crust including the Moho, which geometry is particularly complex in the Alps where European, Adriatic and Ligurian Moho overlap, before moving on to tomography of Alpine subductions.

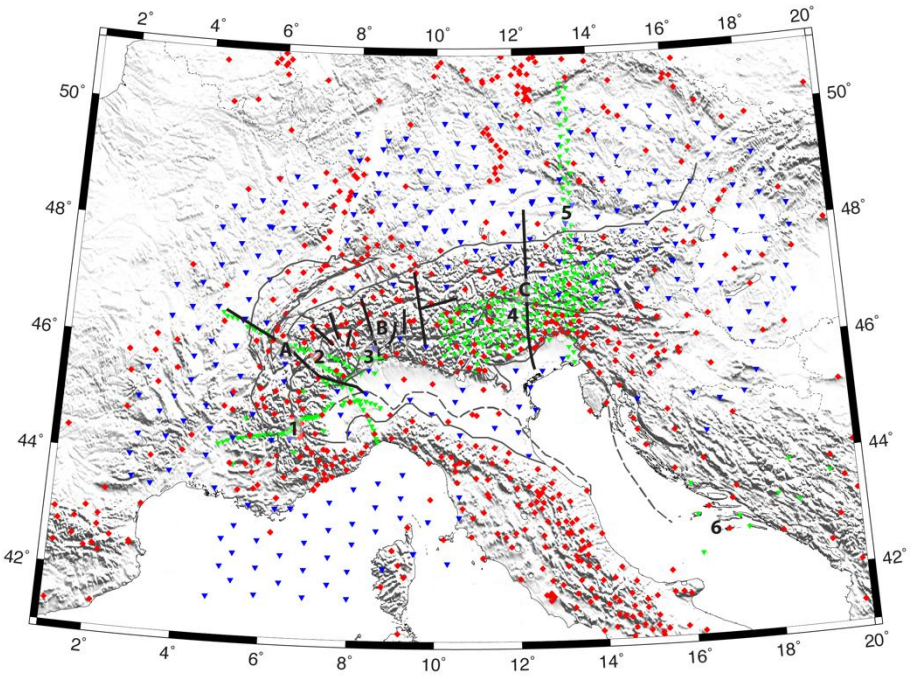

Figure 2.1. *Location map of seismic stations deployed in the Alpine region since 2012. Red diamonds: permanent networks; inverted triangles: temporary experiments; blue: AlpArray seismic network; green: (1) Cifalps, (2) Cifalps-2, (3) Ivrea, (4) Swath-D, (5) EASI, (6) CASE. Thick black lines show locations of controlled-source seismic experiments: (A) ECORS-CROP, (B) NFP-20 and (C) TRANSALP. The main tectonic boundaries are shown as thin grey lines. Some of these deployments are recent and have not yet resulted in publications at the time of writing (Cifalps-2, Ivrea, Swath-D).*

At the time of writing, several temporary experiments including AlpArray, have recently been completed in the Alps and the exploitation of their data is in progress.

A further step towards more reliable and better resolved geophysical models of the Alpine crust and mantle is expected in the coming months and years.

2.1. Probing a very complex crust and crust-mantle boundary

The primary objective of most geophysical investigations of the crust is the crust-mantle boundary, or Moho because it is characterized by a generally abrupt petrological change between granulites of the lower crust (under continents) with P-wave velocity (Vp) of ~6.7 km/s and density (ρ) of ~2.7 10^3 kg.m^{-3}, and peridotites of the upper mantle with Vp≈8 km/s and ρ≈3.3 10^3 kg.m^{-3}. At depth greater than the base of sedimentary basins, the Moho is thus the petrologic discontinuity that is the most accessible to active seismic profiling or passive seismology. Probing the bulk structure of the crust is more difficult due to generally weak seismic wave-velocity and density contrasts. This section begins by reviewing the most widely-used geophysical methods for probing the crustal structure and for mapping Moho depth.

2.1.1. A quick update on crustal exploration methods

Refraction and reflection seismology, with the latter including near-vertical incidence and wide-angle, have been widely used because they are particularly effective for imaging strong velocity contrasts such as the Moho with excellent vertical resolution. They are rather expensive though and hardly compatible with current environmental constraints. As a result, the latest crustal-scale controlled-source (or active) seismic experiments in the Alps are Transalp (Lüschen et al. 2006) in the eastern Alps and the wide-angle experiments of the GéoFrance-3D Alps project in the western Alps (Thouvenot et al. 2007).

Today, crustal imaging is mainly based on passive seismology, using earthquakes and noise recordings. Compared to controlled source seismology (CSS), the signals have a lower frequency and therefore a lower vertical resolution. However, a reasonably dense network of seismic profiles makes it possible to calibrate the depth of the interfaces by comparison with CSS data, while passive seismology provides 3-D constraints and fills the gaps between CSS profiles. The most frequently used methods are described in the following paragraphs.

Receiver function analysis is often used to estimate the depth of the main velocity discontinuities in the crust, particularly the Moho, using the three-component records of teleseismic earthquakes (Vinnik 1977). When the teleseismic P-wave hits an interface from below, part of its energy is converted into a S-wave which is recorded on the horizontal components of the sensor a few seconds after the

P-wave. Calculating receiver functions consists in enhancing the Ps waves (P-to-S converted waves at velocity discontinuities such as the Moho) in the P-wave coda. The arrival time difference between the P wave and a Ps wave converted at a velocity discontinuity depends on the average Vp and Vp/Vs ratio above the discontinuity and on the depth of the discontinuity. The amplitude of the Ps wave depends on the velocity contrast at the discontinuity. As in vertical-incidence seismic reflection, a depth migration is necessary to convert the arrival time difference between the P and Ps waves into depth. It is also required to place the conversion point at its exact position, due to the obliquity of the seismic ray. The simplest depth migration method, named CCP stacking (for common conversion point; Dueker and Sheehan 1997) assumes a flat-layered crust and requires a crustal velocity model. By calculating and migrating the receiver functions at a series of seismic stations aligned along a profile, a CCP migrated section is obtained that in most cases shows the Moho depth variations along the profile. CCP sections are often displayed in a blue to red color scale, where blue corresponds to a velocity discontinuity of decreasing velocity with increasing depth, while red corresponds to a discontinuity of increasing velocity with increasing depth. Care must be taken to interpret these blue and red spots as interfaces and not as areas of high or low seismic velocity. Examples of CCP sections for the Transalp, Cifalps and EASI profiles will be discussed in section 2.3.

Local earthquake tomography (LET; Thurber 1983) consists in inverting arrival times of P (and S) waves generated by local earthquakes and recorded at a seismic array for absolute Vp, Vp/Vs ratio (if S wave arrival times have been picked) and hypocenter parameters (location, origin time). The LET method provides P-wave velocity images of the bulk crustal structure and not only velocity discontinuities. In the Alps, the LET may be inefficient in imaging the lower crust and the Moho because parameters are estimated between earthquake foci, which are mostly located in the upper, brittle crust, and stations (located on the surface).

As outlined in the introduction, ambient-noise tomography (ANT; Shapiro et al. 2005) has the potential to transform any seismic station into a source for other stations. The first step of ANT is to calculate the noise correlations between all station pairs available in the study region. If noise correlations are calculated over a time span long enough to ensure a sufficiently wide distribution of noise sources around the stations, they are dominated by the Rayleigh wave between the two stations. The second step is therefore a surface wave tomography. It involves measuring the group or phase velocity of the Rayleigh wave at different frequencies and inverting the resulting dispersion measurements to estimate a 3-D S-wave velocity model under the station network. As for local-earthquake tomography, ANT provides images of the bulk structure of the crust, in that case in S-wave velocity.

The forward modelling of gravity anomalies, in particular the Bouguer anomaly (onshore) is used to test crustal models derived from other geophysical methods, and geological and petrophysical data (e.g. Lardeaux et al. 2006). Inversion of gravity data can provide additional information provided that a suitable initial model is available. An important step forward will be provided in the next few months by the release of a new, homogeneous gravity database compiled from surface data across the Alpine area by the AlpArray gravity research group (Zahorec et al. 2021). Other methods exist, such as magneto-tellurics (MT), which aims to estimate the conductivity of the subsurface, hence its fluid content; but it has not yet been used in the Alps, at least on a large scale.

2.1.2. Crustal tomography at the scale of the entire Alpine belt

2.1.2.1. A review of Moho models from controlled-source seismology, local earthquake tomography and receiver functions

The first 3-D numerical model of Moho depth under the Alps was built by Waldhauser et al. (1998) from the results of seismic refraction and vertical-incidence reflection profiles. They systematically reviewed all the results, assigned to each reflector portion an uncertainty depending on the signal quality; then they migrated these reflector portions in 3-D before interpolating the data to determine the simplest and smoothest possible surface. Their Moho depth map presented in Fig. 2.2b clearly shows the European Moho underthrusting the Adriatic Moho, which in turn underthrusts the Ligurian Moho. The locations of the vertical offsets between the three Moho surfaces are shown as dotted lines. Note the low density, or even the lack of data available in the south-western Alps or in the eastern Po basin. The Ivrea body at the border between Adriatic Moho and European Moho under the western Alps is not detected.

To complement the CSS (controlled-source seismic) data, Wagner et al. (2012) measured Moho depth in the Vp model of Diehl et al. (2009) derived from a local earthquake tomography (LET). Since this LET uses a large number of arrival times of refracted Pn waves in the uppermost mantle, its resolution is fair down to the crust-mantle boundary. The Moho is approximated by the surface of isovelocity Vp=7.25 km/s and the authors attribute to each depth measurement an uncertainty and a weight that depend in part on the velocity gradient. The interpolation procedure is identical to that of Waldhauser et al. (1998). The resulting map is shown in Fig. 2.2c. The main difference with the map of Waldhauser et al. (1998) in Fig. 2.2b is the sharp rise of the Adriatic Moho to the top of the Ivrea body above the European Moho.

The densification of the permanent seismological networks has enabled the Moho depth maps to be progressively complemented with receiver functions (RF) measurements (e.g. Lombardi et al. 2008; Piana Agostinetti and Amato 2009). Spada et al. (2013) constructed a new Moho map for Italy by combining CSS and RF data in an interpolation similar to the one used by Waldhauser et al. (1998). They used the local earthquake tomographies of Diehl et al. (2009) and di Stefano et al. (2009) to verify the Moho depths obtained by RF and evaluate their uncertainties. The Alpine part of their map is shown in Fig. 2.2d. In the western Alps, their Moho model is identical to that of Wagner et al. (2012) and essentially derived from the LET of Diehl et al. (2009), since CSS and RF data were scarce. On the other hand, it extends further south and includes the Ligurian Sea and the Corsica-Sardinia block. It also covers the eastern Alps where it shows a Moho gap east of 12.5°E (grey-filled area in Fig. 2.2d). This Moho gap is documented by the analysis of PmP waves (P waves reflected by the Moho at critical distance) recorded during the CELEBRATION2000 and ALP2002 CSS experiments (Behm et al. 2007). It is due to lack of data (i.e. PmP reflections) and/or poor data quality.

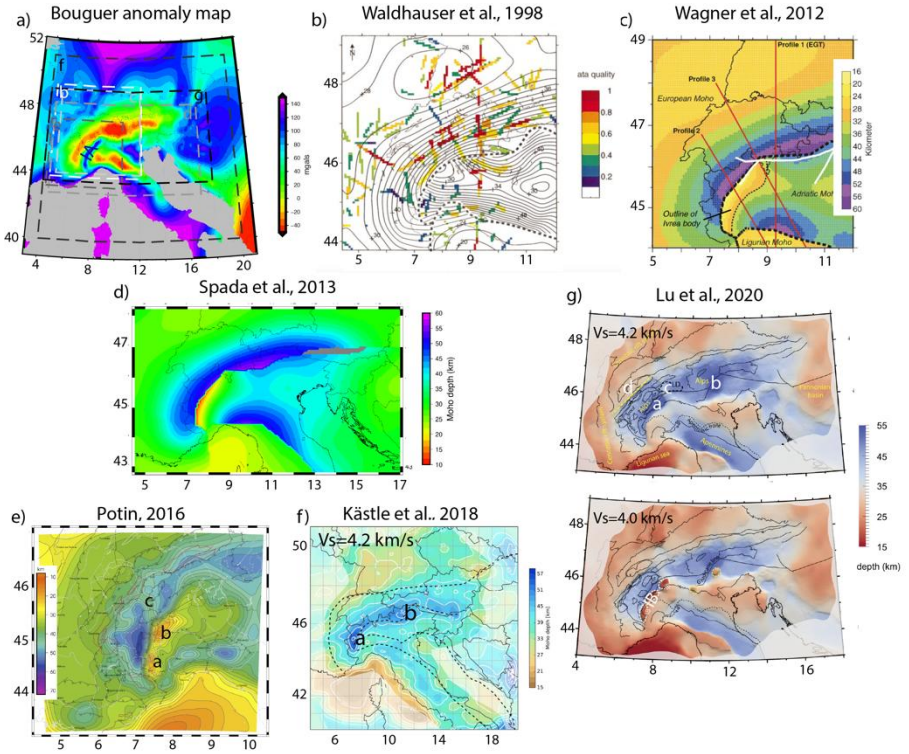

Figure 2.2. *Some depth maps of Alpine Moho, or proxy of Alpine Moho. (a) Bouguer anomaly map shown for comparison (World Gravity Map - 2012, Bonvalot et al. 2012); The areas enclosed by white, grey, black dashed lines and identified by letters (b-g) show the locations of maps displayed in Figures 2.2b-g; IA: Ivrea anomaly. (b) Waldhauser et al. (1998): review and interpolation of seismic refraction and vertical-incidence reflection data; Moho depth mapped as contour lines; the colored line segments show the locations of the CSS data used, with color corresponding to data quality from poor (blue) to high (red); the thick black dotted lines show the locations of Moho steps. (c) Wagner et al. (2012): same CSS data as in (b) supplemented with segments of isovelocity surface Vp =7.25 km/s from the LET of Diehl et al. (2009); the thin black dotted line is the outline of the Ivrea body. (d) Alpine part of Spada et al. (2013)'s map: same as (c) supplemented with receiver function observations and CSS wide-angle data in the eastern Alps; the grey-filled area is the so-called Moho gap of the eastern Alps, where no wide-angle PmP reflection could be detected. (e) Potin (2016): depth of strongest vertical gradient in his Vp model computed by LET in the western Alps. (f) Kästle et al. (2018): depth of isovelocity surface Vs=4.2 km/s in the 3-D Vs model calculated by ambient noise and teleseimic earthquake surface-wave tomography; main tectonic boundaries plotted as thick black dotted lines. (g) Lu*

et al. (2020): depth maps of isovelocity surface Vs=4.2 km/s (top) and Vs=4.0 km/s (bottom) in the Vs model calculated by ambient noise wave-equation tomography; main tectonic boundaries shown as black lines; IB: Ivrea Body; LD: Lepontine dome.

The next Moho model shown in Fig. 2.2e comes from the LET of Potin (2016) in the western Alps. It is to date the best-resolved LET in the western Alps thanks to the comprehensive database used, but it is not published yet. In the central area where the resolution is very good, the Moho depth is estimated from the strongest vertical Vp gradient (with Vp between 7.3 and 7.6 km/s). In more external areas, the map is obtained by averaging the depths of existing models, in particular that of Wagner et al. (2012). In the central region (5.5-9°E; 44-46.5°N), there are faster depth variations than in the very smooth models mentioned previously, including a two-block Ivrea body (labels "a" and "b" in Fig. 2.2e) and an uprising of the European Moho under the Aosta region (label "c"). That particular geometry of the Ivrea body poorly corresponds to the Bouguer anomaly which shows no evidence of the presence of two such differentiated blocks in the anomaly high of the Ivrea body (labelled "IA" in Fig. 2.2a).

2.1.2.2. S-wave velocity models from ambient-noise tomography

Ambient Noise Tomography (ANT) has been applied several times since its emergence in the early 2000s to determine the crustal Vs structure under the Alpine arc. Stehly et al. (2009) used records from 150 permanent stations located mainly in the western and central Alps. This pioneering application to the Alpine region clearly demonstrated the ability of ANT to provide a spatially continuous 3-D Vs model in a region where seismicity is not only moderate but also inhomogeneously distributed. Molinari et al. (2015a) used about the same stations as Stehly et al. (2009) in the Alps, and more stations in Italy. Their Vs model was derived from a non-linear inversion of the group and phase velocities of the Rayleigh wave. This non-linear inversion allowed to explore the solution space in the vicinity of *a priori* models defined by synthesizing existing models, that is EPcrust (Molinari et al. 2011) for the European crust and MAMBo (Molinari et al. 2015b) for the Po basin. This inversion method led to a more robust crustal model than the linear inversion of Stehly et al. (2009). The Moho depth map is an improved version of the very smooth Moho model of Spada et al. (2013) that Molinari et al. (2015a) used as *a priori* model. The lateral resolution of this model remains however inadequate (100-200 km depending on the region) to add significant new constraints to the geological models.

Kästle et al. (2018) combined Rayleigh and Love wave dispersion observations from ambient noise with dispersion data from regional and teleseismic records to compute a Vs model of the crust and upper mantle to 200 km depth. Measurements

on earthquake records complement ambient noise data towards the low frequencies that are sensitive to deeper structures, from the base of the crust to the upper mantle. They used data from a larger number of permanent stations than previous publications, ensuring fairly good coverage of the entire Alpine arc. Like Molinari et al. (2015a), their 3-D model of Vs is computed by stochastic inversion, but they explore a larger set of models with no *a priori*. The resolution of their model (= minimum size of the heterogeneities that the model is able to distinguish) is ~50 km in the upper and middle crust and ~100 km in the upper mantle, over all the Alps. The fast-velocity anomaly of the Ivrea body is as well detected as in the Vp model of Diehl et al. (2009). The depth map of the 4.2 km/s isovelocity surface, used as a proxy for Moho (Figure 2.2f) shows details that were not visible on the very smooth map by Spada et al. (2013) in Fig. 2.2d. The maximum depth of the European Moho is 55 km under the western Alps, just in front of the Insubric line and the Ivrea body ("a" in Fig. 2.2f), and 50 km in the central Alps under the Giudicarie line ("b" in Fig. 2.2f).

A further step in the number of stations used and thus the spatial resolution of the Vs model was taken by Lu et al. (2018) in an ambient noise tomography of Europe using data from nearly 1300 seismological stations, including the first six months of data from the temporary AlpArray network (Hetényi et al. 2018a). The Alps are particularly well covered by this Rayleigh-wave group-velocity data set, with an estimated resolution of 0.3° (~30 km) in the upper crust and 0.9° (~100 km) at Moho depth. The final Vs model resulting from a Bayesian non-linear inversion is probabilistic, in the sense that it includes the probability density on the values of Vs, but also on the depth of the interfaces including Moho. Lu et al. (2020) further improved the Vs model of Lu et al. (2018) in the Alpine region by inverting ambient noise phase dispersion data based on elastic waveform simulation. Unlike conventional ANT methods that rely on ray theory and apply a point-by-point 1-D depth inversion of dispersion data for S-wave velocity, such a wave-equation tomography accounts for 3-D and finite frequency effects. The resulting 3-D Vs model is therefore more in line with the basic principles of seismic wave propagation. Figure 2.2g shows two depth maps of isovelocity surfaces Vs=4.2 km/s (top) and Vs=4.0 km/s (bottom) in the Vs model of Lu et al. (2020). The isovelocity surface 4.2 km/s (also used by Kästle et al. 2018; Fig. 2.2f) is a good proxy for Moho everywhere except for the Ivrea body. The Ivrea body shows up on the 4.0 km/s depth map (dashed white line labelled "IB" in Fig. 2.2g-bottom) because it is made up of serpentinized Adriatic mantle whose S-wave velocities can be as low as 3.6-3.8 km/s (e.g. Reynard 2013). The 4.2 km/s map shows significant variations in the maximum depth of the European Moho along the arc, with two maxima below the Sesia zone in the western Alps (52-54 km; "a" in Fig. 2.2g-top) and below the Giudicarie Line (54-56 km; "b" in Fig. 2.2g-top) in the central-eastern Alps and a

high point below the Lepontine Dome (40-42 km; “c” in Fig. 2.2g-top). The 4.2 km/s isovelocity depth map also shows a ~8 km abrupt step that closely follows the northwestern boundary of the external crystalline massifs of the western Alps (yellow dashed line labeled “d” in Fig. 2.2g-top). This previously unknown structure coincides with the disappearance of the European Moho in the ECORS-CROP vertical seismic reflection section. Its rectilinear shape and SW-NE orientation suggest that it may be related to a Variscan lithospheric discontinuity. The Ivrea body is visible at 20-22 km depth on the 4.0 km/s map (“IB” in Fig. 2.2g-bottom), with a geometry that roughly corresponds to that of the positive Bouguer anomaly (“IA” in Fig. 2.2a). The depth of the 3.6 km/s isovelocity surface (not shown here) is shallower than 10 km in some parts of the Ivrea body, in better agreement with the depth to the top of the high-velocity body observed with early refraction seismic experiments (Closs and Labrouste 1963).

2.1.3. Crustal structure imaged along seismic transects across the Alps

Seismic arrays provide 3-D images of the lithospheric structure whose resolution is at best of the order of magnitude of the distance between stations, i.e. ~40-50 km under most of the Alps (with the AlpArray seismic network). Geological structures are usually smaller in size. In order for the resolution of seismic tomography to tend towards the resolution of the geological map, sensor arrays must be made denser. For this reason, several dense temporary seismological experiments, with stations spaced 5 to 15 km apart, have been deployed along cross-chain profiles in the last ~20 years. The disadvantage of these experiments is that they usually only provide 2-D sections of the subsurface. However, deploying sensor arrays a few kilometers apart over a significant area is still a logistical and, above all, a financial challenge. The Swath-D experiment of the 4D-MB project (Mountain Building in 4 dimensions, German component of AlpArray, http://www.spp-mountainbuilding.de) is such a sensor array (Heit et al. 2017, 2018). 163 broadband sensors were installed in Austria and Italy from 2017 to 2019 in a rectangle of ~330x120 km^2 with a spacing of 12-15 km between stations (labelled “4” in Fig. 2.1). The main objective of Swath-D is to study the assumed polarity flip of the subduction between central and eastern Alps and the Moho "hole" (Spada et al. 2013 and Fig. 2.2d). Results are expected after the publication of this review.

2.1.3.1. Recent results on the subduction channel of the western Alps (Cifalps and AlpArray experiments)

The temporary Cifalps experiment (Zhao et al. 2016a; see location in Fig. 2.1, label “1”) involved a profile of 46 stations with 5-10 km spacing across the south-western Alps from the southern Rhône valley (France) to the Po basin (Italy), and 10

offline stations to complete the coverage of permanent networks. The main objective of Cifalps was to study the structure of the Alpine subduction channel under the Dora Maira massif where the first mineralogical evidence of continental subduction was discovered by Chopin (1984) in the form of coesite inclusions in garnets. Coesite is a (U)HP/HT mineral formed by burying continental crust at a depth of 90 km or more.

Before Cifalps, two seismic experiments had been carried out in the late 1990s in the southwestern Alps in the framework of the French GeoFrance-3D program. A temporary seismic array provided data for a LET focused primarily on the Ivrea body (Paul et al. 2001), which was the basis for a joint geological-geophysical interpretative crustal-scale cross-section (Lardeaux et al. 2006). A wide-angle experiment provided new data on the depth of the European Moho and failed to confirm the existence of the Briançonnais mantle flake proposed on the basis of the ECORS-CROP experiments (Thouvenot et al. 2007).

Using the receiver functions from the Cifalps data, Zhao et al. (2015) found P-to-S converted waves on a velocity discontinuity 75-80 km below the western edge of the Po plain (labelled “a” in Fig. 2.3a) in the continuity of the European Moho which is clearly visible further west (“b” in Fig. 2.3a). They interpreted these signals as the first seismological evidence of the presence of the European Moho at a depth of 75-80 km, thus of subduction of the continental lithosphere under the Alps. A set of Ps conversions of negative polarity and high amplitude (blue color in Fig. 2.3a, labelled “c”) is detected at a depth of 20-40 km under the Dora Maira massif and the western Po plain. The negative polarity indicates that signals are produced by a velocity discontinuity where the velocity decreases with increasing depth. Combining geological data and models, petrophysical data, gravity and seismological modelling, Zhao et al. (2015) proposed an interpretive crustal scale section that includes a thick suture zone under the Dora Maira massif (Fig. 2.3c). This zone is characterized by velocities decreasing with increasing depth below the Ivrea body. It indicates that the European lower crust underthrusts the Adriatic mantle, almost vertical to the place where coesite was discovered by Chopin (1984).

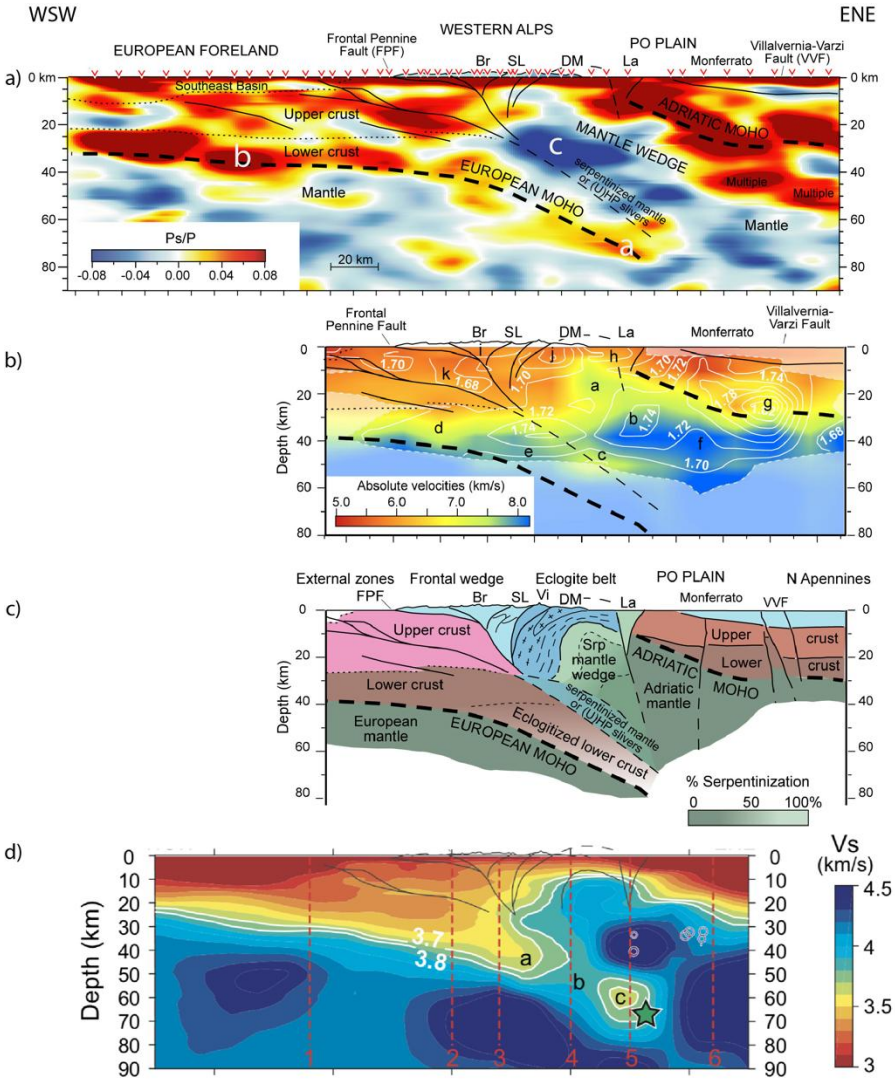

Figure 2.3. *Depth sections of seismic parameters along the Cifalps profile (southwestern Alps, location in Fig. 2.1, labelled "1"), and geological interpretation. (a) Result of receiver function analysis: common conversion point (CCP) section of Zhao et al. (2015) where the blue and red patches show converted waves on interfaces with velocity increasing (red) or decreasing (blue) with increasing depth; (b) Result of local earthquake tomography (LET): P-wave velocity model of Solarino et al. (2018) and contours of Vp/Vs ratio (white lines); (c) Interpretive geological section constructed from (a) and (b) (modified from Solarino et al. 2018); (d) Result of*

transdimensional inversion of Rayleigh wave group velocity dispersion data: S-wave velocity model of Zhao et al. (2020); the small white circles are hypocenters of microearthquakes located in the vicinity of the section. Br: Briançonnais, DM: Dora Maira, FPF: Frontal Pennine Fault, La: Lanzo, SL: Schistes Lustrés, Vi: Viso, VVF : Villalvernia-Varzi Fault.

The geophysical and geological model of the suture zone (or subduction channel) under Dora Maira has been refined by the LET of Solarino et al. (2018; Fig. 2.3b). This paper shows that the (U)HP Dora Maira dome is, at a depth of 10 km, directly in contact with partially serpentinized peridotites of the Ivrea body (Vp~7.5 km/s; Vp/Vs=1.70-1.72; labelled "a" in Fig. 2.3b). These serpentinites extend down to the top of the eclogitized European lower crust ("e" in Fig. 2.3b). Towards the east and between 20 and 50 km deep, the serpentinized peridotites are in contact with the dry peridotites of the Adriatic mantle (Vp~8 km/s; Vp/Vs>1.74; labelled "b" in Fig. 2.3b) from which they are separated by a quasi-vertical lithospheric and seismogenic fault marked by microearthquakes (red circles in Fig. 2.3d). The region marked "c" in Fig. 2.3b has lower Vp (Vp ~7.0-7.5 km/s) than the serpentinized peridotites of the Ivrea body. These could be more serpentinized peridotites than those of the Ivrea body and/or (U)HP continental rock slivers. At greater depth, the area marked "e" has higher Vp (~7.7 km/s) that is interpreted as eclogitized European lower crust. The seismic structure of the subduction channel can be seen here from the surface to the top of the eclogitized lower crust over a thickness of almost 50 km. The decrease in velocity between the Ivrea body (Vp~7.5 km/s; "a" in Fig. 2.3b) and the more strongly serpentinized peridotites (and/or (U)HP slivers) located below it (Vp ~7.0-7.5 km/s; "c" in Fig. 2.3b) could explain the negative polarity of the Ps-converted waves in the CCP section ("c" in Fig. 2.3a), provided that the S-wave velocities undergo the same change as Vp.

The objective of Zhao et al. (2020) was precisely to measure Vs in the subduction channel of the western Alps. They calculated a probabilistic Vs model in the region of the Cifalps profile by transdimensional Bayesian inversion of the Rayleigh wave dispersion measurements of Lu et al. (2018). There is no *a priori* constraint (or very few *a priori* constraints) on the model in this type of inversion and all parameters, for example the number of model layers, are estimated to best fit the data. The computations are much more cumbersome than in more classical inversions, but the velocity values resulting from such an inversion are more reliable than from other methods that require regularization of the inverse problem by *ad hoc* parameters.

The cross-section in the Vs model of Zhao et al. (2020) is shown in Fig. 2.3d. It shows a thick body of slow velocities (Vs=3.6-3.8 km/s; labelled "c" in Fig. 2.3d) at

50 to 70 km depth along the suture zone between the Adriatic mantle wedge above and the eclogitized lower crust and European mantle below. The decrease in Vs with depth under the Ivrea body is much clearer than in the Vp model of Solarino et al. (2018) whose resolution is not good beyond 50-60 km depth. Zhao et al. (2020) ascribe these very low velocities to serpentinites along the subduction channel based on laboratory velocity measurements and petrological and mineralogical data. The low viscosity of the serpentinites gives them an important role in the processes associated with continental subduction, both in the burial and exhumation of HP/HT metamorphic rocks (e.g. Guillot et al. 2009).

2.1.3.2. Recent results on the eastern Alps (TRANSALP and EASI experiments)

The eastern Alps have been traversed by two seismic profiles, TRANSALP and EASI. TRANSALP (1998-2001) was running north-south at 12°E longitude, and it crossed the Tauern Window between the Molasse Basin to the north and the Dolomites to the south ("C" in Fig. 2.1). The experiment combined a vertical-incidence reflection seismic profile (Lüschen et al. 2006) and passive imaging with a temporary seismic array installed along the same transect (Kummerow et al. 2004). The CSS component of TRANSALP was the first reflection seismic profile in the eastern Alps, and the only one to date. Installation of seismological stations along the CSS profile enabled a very interesting comparison between the line-drawing of the CSS profile and the CCP section from the receiver function analysis (Fig. 2.4a). Fig. 2.4a shows that both methods image similar structures, with obviously much better vertical resolution for seismic reflection profiling. However, Kummerow et al. (2004) note a disagreement on the geometry of the Adriatic Moho, which is clearly horizontal at a depth of 40 km on the CCP section (red spot under the Dolomites in Fig. 2.4a), whereas the line drawing of the CSS section shows a set of reflectors with an envelope that seems to dip northward and join the European Moho at a depth of ~55 km (black line segments in Fig. 2.4a). They propose that the better vertical resolution of the reflection CSS profile allows to image a pervasive deformation fabric in-between the European and Adriatic Moho while the receiver functions give access to the Moho (as the velocity discontinuity between crust and mantle) on a large scale. In any case, the European lithosphere appears to subduct beneath the Adriatic lithosphere.

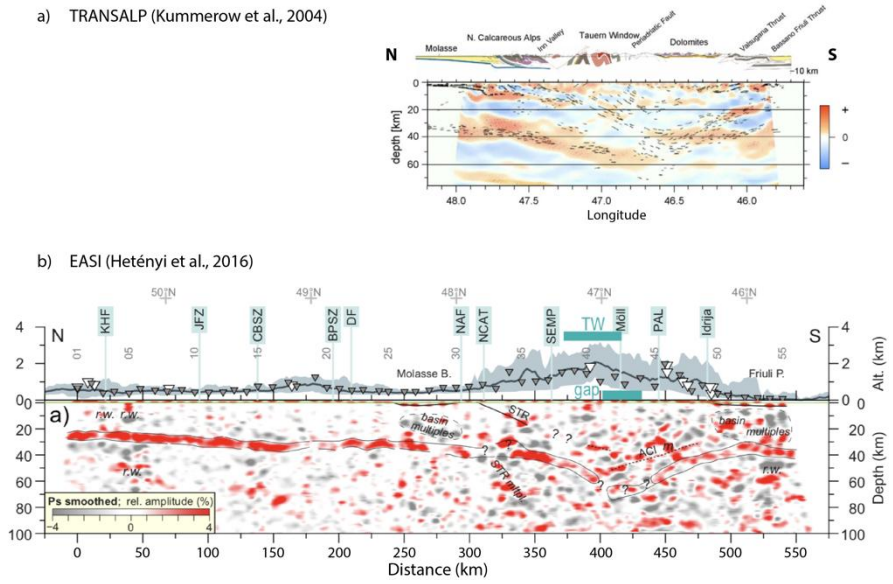

Figure 2.4. *Seismic imaging results across the eastern Alps. (a) Transalp experiment (location in Fig. 2.1, label "c"): line-drawing of the vertical-incidence seismic profile (thin black line segments) and receiver function CCP section (modified from Kummerow et al. 2004); (b) EASI experiment (location in Fig. 2.1): receiver function CCP section by Hetényi et al. (2018b). ACI: Adriatic Crustal Interface, BPSZ: Bavarian Pfahl Shear zone, CBSZ: Central Bohemian Shear Zone, DF: Danube Fault, JFZ: Jáchymov Fault Zone, KHF: Krušné Hory Fault, NAF: Northern Alpine Fault, NCAT: Northern Calcareous Alps Thrust, PAL: Periadriatic Line, SEMP: Salzach-Ennstal-Mariazell-Puchberg fault, STR: Sub-Tauern Ramp, TW: Tauern Window, r.w.: ringing waveform.*

The EASI profile (AlpArray Seismic Network, 2014) is a long passive seismic profile located at 13.3°E longitude from the Bohemian massif in the north to the Adriatic coast in the south ("5" in Fig. 2.1). It crosses the Moho gap documented in particular by Spada et al. (2013) (see section 2.1.2.1 and Fig. 2.2d) south and east of the Tauern Window. The CCP section computed by Hetényi et al. (2018b) is shown in Fig. 2.4b. The Ps converted wave on the European Moho in the north is clearer and laterally more continuous than that of the Adriatic Moho in the south. It is hardly detectable in the suture area under the Tauern window (TW). Hetényi et al. (2018b) carried out a very detailed analysis of receiver functions, including waveform inversion, to propose a model in which the Adriatic Moho underthrusts the European Moho to a depth of 70 km. They propose that the contact zone is

characterized by low-amplitude converted waves (marked with "?" at 60-70 km depth in Fig. 2.4b) produced by a transitional Moho where velocity gradually increases over ~20 km of thickness. Since this transitional Moho can only be detected by low-frequency (and long-wavelength) waves, it is invisible to seismic reflection, which may explain the Moho gap.

Qorbani et al. (2020) used ambient-noise tomography and part of the EASI dataset to compute a crustal 3-D shear-wave velocity model in the area [46°N-48°N; 9°E-17°E] centered on the Tauern Window. As the model is restricted to a maximum depth of 40 km, it provides no information on the contact zone between the European Moho and the Adriatic Moho. The high velocities associated with the metamorphic rocks that form the Tauern Window at shallow depth extend to the bottom of the model at 40-km depth. A comparison is made between a vertical section through the Vs model along the TRANSALP line and a crustal-scale geological cross-section. The boundary between high and low velocities documented by the Vs section is in good agreement with the geological boundaries assumed for the Tauern Window to 10-km depth, but it does not correspond to any geological boundary at 10-30 km depth. Qorbani et al. (2020) suggest interpretations for the Vs boundary, such as a post-nappe metamorphic front to the south of the Tauern Window. This example confirms that such tomographies have a great potential to extend geological maps at depth and in 3-D. It also shows that geological models have to be reconsidered in the light of the results of seismic tomography.

2.2. Probing subduction slabs and mantle fabrics

2.2.1. Subduction slabs

As stated in the introduction, positive Vp anomalies of typical subduction slab geometries in the upper Alpine mantle have been known since the 1990s (Babuška et al. 1990; Cattaneo and Eva, 1990; Spakman, 1990, 1991). The tomographies of Piromallo and Morelli (2003) at the scale of the whole Euro-Mediterranean region and of Lippitsch et al. (2003) in the Alps were breakthroughs in terms of both the quantity and quality of the data used. The teleseismic tomography of Lippitsch et al. (2003) showed a northeastward dip of the fast-velocity anomaly under the eastern Alps, while the fast-velocity slab dips southeastward under the central and western Alps. They interpreted these anomalies as traces of lower continental lithosphere, with the European lithosphere being the lower plate in the western and central Alps and the Adriatic plate the lower plate in the eastern Alps. Interpretation of anomalies as continental rather than oceanic in origin is not based on a difference in the seismic image. The oceanic crust has a different structure (thickness, lithology and therefore seismic velocity) from that of the continental crust, which makes it

possible to distinguish them by seismic tomography. This is not the case of the lithospheric mantle which has similar properties for the two types of lithosphere. The interpretation of Lippitsch et al. (2003) was therefore based on the comparison between the length of the high-velocity slabs and the shortening values estimated by structural geology.

The change in subduction polarity along strike, as well as the highly segmented aspect of Alpine slabs have been the targets of several recent tomographies. They have benefited from the development of permanent networks and the opening of databases. Upper mantle tomography has not benefited as much as crustal tomography from the methodological innovations related to the use of ambient noise correlations. We saw in section 2.1.1 that ambient noise tomography can be used to perform surface-wave tomography without earthquakes. However, the empirical Green functions reconstructed by noise correlation have the same frequency content as the microseismic noise, so most of their energy is concentrated between 5 and 30s period. They are therefore only slightly sensitive to upper mantle depths. As Kästle et al. (2018) have done, the surface wave spectrum can be extended to lower frequencies by using records of teleseismic events to illuminate the upper mantle; but the horizontal resolution of surface wave tomography remains limited. The most widely used method for imaging the upper mantle remains teleseismic tomography. The main limitation is vertical resolution, since teleseismic tomography uses arrival times of P (or PKP, etc.) waves that travel through the mantle in near-vertical rays. Its horizontal resolution depends on the station density. Input data of teleseismic tomography are most often travel time differences (residuals) between stations of an array measured for a set of teleseismic earthquakes. Therefore, the values of velocity anomaly (dVp/Vp) resulting from the inversion at a given depth refer to an unknown horizontally averaged Vp. They cannot be used to reconstruct the absolute Vp model.

FWI (Full Waveform Inversion) on a regional scale has not yet demonstrated its full potential in applications to the Alps (on a regional scale: Beller et al. 2018; on a continental scale: Zhu et al. 2015, Fichtner et al. 2018). In a recent review of published tomographies of the upper mantle under the Alps, Kästle et al. (2020) compares the results of Zhu et al. (2015) and Fichtner et al. (2018) with those of different teleseismic tomographies (their Figures S1 and S2 in the supplementary information file). Horizontal resolution is clearly not (yet) at the level of what can be achieved by teleseismic tomography, but new results are expected in the near future with AlpArray data (Paffrath et al. 2020).

I return in the following to a series of questions raised in Lippitsch et al. (2003).

2.2.1.1. With or without slab tears?

The tomography of Lippitsch et al. (2003; Fig. 2.5a, d) shows on all depth slices from 90 to 240 km depth three well-individualized fast-velocity anomalies along the arc, of size ~150 km x 150 km. At a depth of 200 km (Fig. 2.5d), they are located under the western Po plain in the western Alps, slightly west of the Giudicarie line in the central Alps, and northeast of the eastern end of the Tauern Window in the eastern Alps. The anomaly amplitudes are similar at 200 km depth; but at depths shallower than 150 km, the western anomaly is attenuated, and even positive at 120 km. The along-dip amplitude change in the western Alps is clearly visible in the cross-section of Fig. 2.6a, while the dip of the deep high-velocity slab is ~50°. Lippitsch et al. (2003) interpreted this attenuation of the amplitude of the positive anomaly at 100-150 km as an indication of a breakoff of the European (Alpine) slab in the W-Alps. Subsequently, this hypothesis has been used in a significant number of publications, for example to explain the rapid exhumation measured in the western Alps since 2 Ma (Fox et al. 2015), or the present fast uplift rates measured by GNSS in the highest regions of the western Alps (Nocquet et al. 2016; Sternai et al. 2019).

Every teleseismic arrival time tomography published since Lippitsch et al. (2003) shows a continuous fast-velocity slab across the upper mantle of the western Alps (Koulakov et al. 2009; Zhao et al. 2016b; Hua et al. 2017; cf. Fig. 2.5 and 2.6b-c). It is also continuous in the tomography of Piromallo and Morelli (2003), as well as in the tomographies of the crust and mantle by FWI of Zhu et al. (2015) and Fichtner et al. (2018), even if an argument can be made about the low resolution of the latter two models. As mentioned earlier, teleseismic tomography has a better resolving power in the horizontal direction than in the vertical direction, due to the near-vertical incidence of rays from teleseismic sources. Horizontal resolution depends primarily on the spatial coverage of the station array and the distribution of earthquakes around the study region, i.e. on the dataset used. In the western Alps, the low vertical resolution problem is further enhanced by the presence of the Ivrea body at crustal depths. Its anomalously fast velocities (as compared to normal continental crust) generate arrival time advances that are difficult to separate from the time advances produced by the subduction slab in the mantle. To prevent the Ivrea body anomaly from leaking vertically and masking a possible slab breakoff, an optimal ray crisscrossing is required in the uppermost mantle, i.e. a dense network of stations and a uniform distribution of earthquakes in back-azimuth. The second condition is never met in the Alps as very few events have backazimuths between 100° (ESE) and 250° (WSW). In addition to data from the permanent networks, Zhao et al. (2016b) used data from the temporary Cifalps network, with an average interstation distance of 7 km and 5 stations located directly above the Ivrea body (see location in Fig. 2.1, label “1”). They used finite frequency tomography, which

is more in line with the physics of wave propagation since it takes into account the sensitivity of waves to the medium around the ray, at a distance depending on the frequency of the used signals. Conventional teleseismic tomography (known as ACH in reference to the authors of the reference publication, Aki et al. 1976) uses infinite frequency approximation and considers that arrival times are only influenced by media traversed by infinitely thin rays. Zhao et al. (2016b) avoid vertical smearing thanks to the station density along the Cifalps profile and, to a lesser extent, thanks to finite frequency tomography. Using synthetic examples, they demonstrate that, under the Cifalps profile, their tomography can reconstruct a fast-velocity anomaly located in the crust (akin to Ivrea body) with negligible leakage to mantle depths. If a slab breakoff did exist beneath the western Po Plain, I am convinced that it would be detected by the tomography of Zhao et al. (2016b).

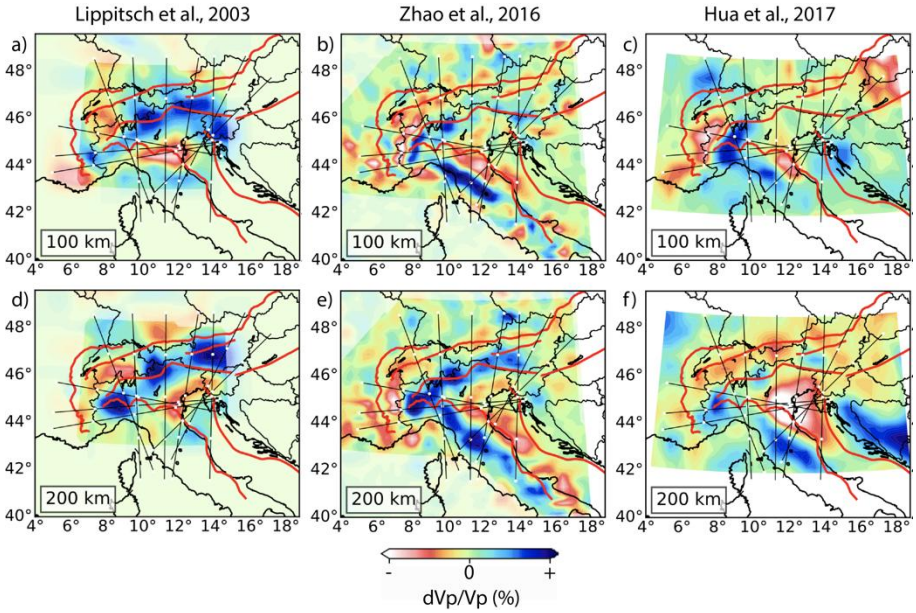

Figure 2.5. *Comparison of depth slices at 100 km (top) and 200 km (bottom) in three dVp/Vp tomographic models published for the Alpine mantle. (a), (d): Lippitsch et al. (2003); (b), (e): Koulakov et al. (2009); (c), (f): Zhao et al. (2016b). The boundaries of the color scales are ±5% for (a) and (d), ±3% for (b) and (e), and ±4% for (c) and (f). Thick red lines show the main tectonic boundaries. Thin black lines show the locations of cross-sections, three of which are shown in Fig. 2.6. Modified from Kästle et al. (2020, supplementary information).*

Most tomographies have applied crustal corrections calculated in an *ad hoc* model, e.g. the model of Waldhauser et al. (2002) for Lippitsch et al. (2003), to

overcome the leakage problem of the Ivrea body anomaly in the mantle. Therefore, the result of the tomography is not only determined by the observations, but also by the *a priori* model.

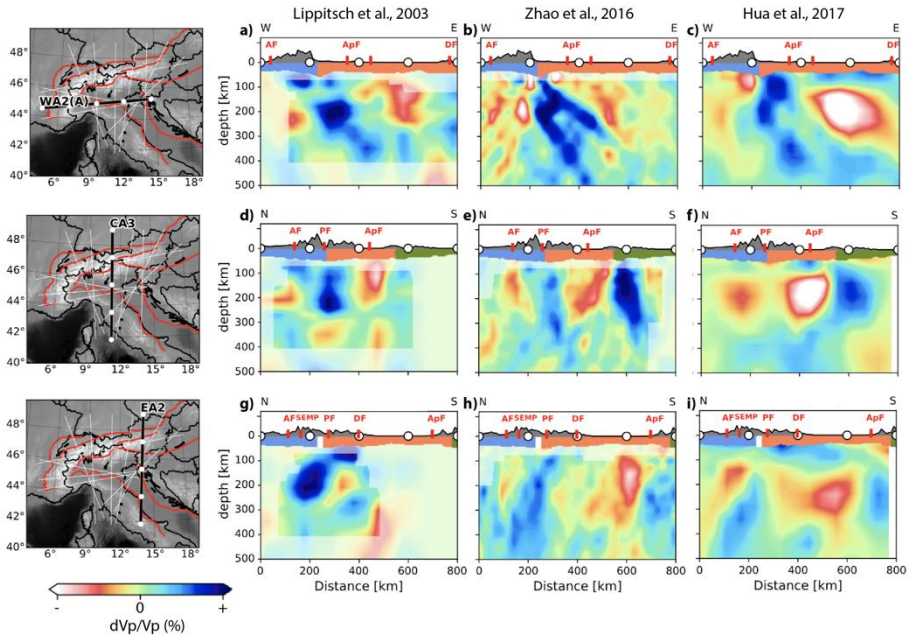

Figure 2.6. *Comparison of vertical cross-sections through the tomography models of: (a), (d), (g) Lippitsch et al. (2003), (b), (e), (h) Koulakov et al. (2009), and (c), (f), (i) Zhao et al. (2016b). Locations of cross-sections are shown on the right: western Alps (top), central Alps and transition to Apennines (middle), eastern Alps (bottom). The boundaries of the color scales are ±5% for (a), (d), (g) and ±3% for (b-c), (e-f) and (h-i). Unresolved regions are masked with lighter colors. Crustal thickness profiles from Spada et al. (2013) are shown on top of each section, with blue color corresponding to European crust, orange to Adriatic crust, green to Ligurian-Tyrrhenian crust and white to the slab gap in the eastern Alps. Red lines and annotations are the main tectonic boundaries: AF: Alpine Front, ApF: Apenninic Front, DF: Dinaric Front, PF: Periadriatic Fault, SEMP: Salzach-Ennstal-Mariazell-Puchberg fault. Modified from Kästle et al. (2020, supplementary information).*

Kästle et al. (2020) provides a comprehensive review of recent tomographic models of the upper mantle under the Alps. In addition to the body-wave tomographies mentioned above, they discuss the contributions and limitations of the surface-wave tomography of Kästle et al. (2018) that combines observations of

Rayleigh wave phase velocities from noise correlations (for the crust, see section 2.1.2.2) and teleseismic recordings for the mantle. Surface-wave tomography has better vertical than horizontal resolution and can therefore complement body-wave tomography. The Vs model of Kästle et al. (2018) covers depths shallower than 200 km. They find a fast anomaly limited to the first 100-km depth in the western Alps, whereas it extends to 150-200 km in the central Alps. They also detect a fast mantle anomaly under the Po plain, which they ascribe to the Apenninic subduction. Other tomographies however show rather slow velocities along this same section under the Po plain. The surface wave tomography of Lyu et al. (2017) along the Cifalps profile finds fast velocities down to 200 km (base of the model) under two mini-arrays of the western Po plain, in contradiction with the results of Kästle et al. (2018).

The teleseismic full-waveform inversion of Beller et al. (2018) on Cifalps data detected a low Vs anomaly between 70 and 120 km depth that they propose to interpret as a trace of the breakoff of the western Alps slab. This anomaly is more superficial than those of Lippitsch et al. (2003) or Kästle et al. (2018). Moreover, the slow anomaly is located at the edge of the European Moho detected by receiver functions by Zhao et al. (2015). It is therefore more likely related to subduction of the European crust or to (U)HP rocks and/or serpentinites in the subduction channel (Zhao et al. 2020).

The AlpArray data will certainly provide decisive elements on the existence or absence of slab breakoffs in the western Alps. The preliminary results of the teleseismic tomography of Paffrath et al. (2020) rather point towards a vertically continuous slab in the western Alps as in the other parts of the chain.

2.2.1.2. Relationship between the Alpine and Apenninic slabs

The lack of continuity between the southwestern end of the Alpine slab and the northwestern end of the Apenninic slab is in line with recent kinematic reconstructions in the Mediterranean (e.g. Jolivet and Faccenna, 2000; Vignaroli et al. 2008; Dumont et al. 2012; Malusà et al. 2015). The Apenninic subduction retreated eastward from the end of the Oligocene, while the Adriatic microplate was still moving northward with respect to Europe, resulting in continental collision in the Alps (Malusà et al. 2016).

The two subductions of the European lithosphere under the western Alps and the Adriatic lithosphere under the northern Apennines are very close and have opposite dips, towards the East for the Alps and towards the Southwest for the Apennines (e.g. Piromallo and Morelli, 2003). Imaging the deep structure at the intersection of two subductions of opposite dips and two arcuate mountain ranges is a real challenge for seismic tomography. The cross-sections of Fig. 2.6d (Lippitsch et al.

2003) and Fig. 2.6e (Koulakov et al. 2009) only display the southward dipping Alpine slab. The question of the relationship between Alpine (European) and Adriatic (Apenninic) slabs was addressed by Vignaroli et al. (2008) on the basis of the tomography of Piromallo and Morelli (2003), and the reinterpretation of geological data and paleotectonic reconstructions. Vignaroli et al. (2008) shows a N-S section in model PM0.5 (Piromallo and Morelli, 2003) across the central and Ligurian Alps that displays the south-dipping Alpine slab under the central Alps, but no fast anomaly to the south. The two fast anomalies of the Alpine and Apenninic slabs seem horizontally disconnected on a NW-SE section. By combining this information with geological arguments and paleotectonic reconstructions, Vignaroli et al. (2008) proposes that the retreat of the Apenninic slab induced an outward toroidal asthenospheric flow from below the retreating Apenninic slab through the gap between the two slabs. This asthenospheric flow in turn forced the general westward retreat of the Alpine slab. The more recent teleseismic tomography by Giacomuzzi et al. (2011) shows that fast anomalies located beneath the northern Apennines merge with the fast anomaly beneath the western Alps between 140 and 180 km depth beneath the Ligurian Alps.

Zhao et al. (2016b) showed that the two fast anomalies that remain distinct to 160 km coalesce from 180 km downward, where the north-dipping slab fragment at the northern end of the Apennine slab comes into contact with the European slab (Fig. 2.6f). Zhao et al. (2016b) question the origin, Alpine or Apenninic, of this surprisingly north-dipping high-velocity anomaly observed at depths <200 km along the Alps-Apennines transition zone (Fig. 2.6f). Its location in the continuation of and at the northern end of the Apennine slab is more in line with an Apenninic origin. The northernmost tip of the Apenninic slab would then have been strongly overturned from a vertical to southwestward dip to a northward dip. Zhao et al. (2016b) rather favor an Alpine origin for the short North-dipping fast-velocity slab fragment because it is located beneath the Ligurian Alps that were structured by Alpine subduction (Malusà et al. 2015) and rotated counterclockwise by up to 90° since the Oligocene (e.g. Maffione et al. 2008). In this case, the southernmost tip of the European slab initially dipping to the east would have rotated to a northward dip while maintaining its dip angle during rotation.

Independently of the origin of the shallow slab fragment, the proposal by Vignaroli et al. (2008) of a toroidal asthenospheric flow at the northern end of the Apennine slab is incompatible with the close contact between the two slabs in the model by Zhao et al. (2016b). This issue will be further discussed in section 2.2.2 on seismic anisotropy.

2.2.1.3. Northeast-dipping slab in the E-Alps

Lippitsch et al. (2003) first imaged a gap between the high-velocity anomaly of the central Alps and the one of the eastern Alps, coinciding with a strong dip change from southeastward in the central Alps to northeastward in the eastern Alps (Fig. 2.6g). They proposed that the Adriatic mantle lithosphere subducts northeastward beneath the European plate. This northeastward dip, though closer to vertical, was later confirmed by the tomographies of Koulakov et al. (2009; Fig. 2.6h), Zhao et al. (2016b; Fig. 2.6i), Hua et al. (2017). The teleseismic tomography by Mitterbauer et al. (2011) displays a steeply to vertically dipping slab below the eastern Alps, that they interpret as European lithosphere unlike Lippitsch et al. (2003) and other publications cited above. For Koulakov et al. (2009), the polarity of the slab is unclear, and both the Eurasian and Adriatic plates appear to be connected to the high-velocity body (Fig. 2.6h).

An important question that can help to understand the origin of the polarity reversal is its precise location along the arc in the tomographic studies that document it. In Zhao et al. (2016b), Figures 2.5c and 2.5f show that the high-velocity anomalies at 100 km and 200 km coincide with the Periadriatic fault (thick red line) west of longitude 13°E, while east of 13°E, the anomaly at 200-km depth is shifted northward by ~70-80 km with respect to the anomaly at 100-km depth. The slab polarity change from vertical to northeastward is therefore located at ~13°E longitude. Zhao et al. (2016b) interpret the northeastward dipping anomaly as Adriatic mantle lithosphere and they link it to the Dinaric slab. The less well-resolved tomography by Lippitsch et al. (2003) shows a broad gap between the central Alps slab and the eastern Alps slab, and a northward shift of ~70-80 km between the anomaly at 100 and 200 km (Figures 2.5a, 2.5d). The slab polarity reversal is located in the slab gap between 12°E and 13°E. Therefore, the change in slab dip between the central Alps and the eastern Alps is located at ~13°E longitude in the two publications that document it.

To summarize, all teleseismic tomographies since Lippitsch et al. (2003) show a vertical or steeply northeast-dipping high-velocity anomaly beneath the eastern Alps east of ~13°E. This polarity change is confirmed by the receiver-function cross-sections along the TRANSALP line (12°E), where the European lower crust seems to underthrust the Adriatic lower crust (Fig. 2.4a), and along the EASI line (13.3°E) where the Moho shift appears to be in the opposite direction, with Adria underthrusting Europe (Fig. 2.4b). To move forward on the issue of the nature of the high-velocity slab, European or Adriatic, seismic tomography results should be compared with geological data, such as shortening estimates (e.g. Kästle et al. 2020), and hypotheses should be tested by geodynamic modeling.

2.2.2. Mantle fabrics imaged by seismic anisotropy

Only azimuthal anisotropy will be considered here. A medium is azimuthally anisotropic when its seismic velocity depends on the wave propagation (or polarization) direction. Azimuthal anisotropy in the mantle is mostly attributed to strain-induced lattice-preferred orientation of olivine crystals (Nicolas and Christensen, 1987). It is therefore a proxy of mantle deformation, and/or mantle flow. As the crust has a more heterogeneous mineralogical composition than the mantle, crustal anisotropy may be caused by preferentially aligned joints or microcracks in fault gouges for example, by thin layering in sediments, or by highly foliated metamorphic rocks. The most often used marker of seismic anisotropy is shear-wave splitting (SWS) of core-refracted phases, mostly SKS and/or SKKS from teleseismic earthquakes (Silver and Chan, 1991). The crustal contribution to the SWS observations from SK(K)S phases is a question of debate as the measurement integrates the effect of all sources of anisotropy along the raypath. This question is quickly resolved in most publications by considering that the delay time between the two split waves, namely the one polarized in the fast direction and the one polarized in the slow direction, which is often larger than 1 s, is too large for anisotropy to be confined to the crust. Fry et al. (2010) and Schippkus et al. (2020) are the only publications to-date that infer azimuthal anisotropy in the crust, for Switzerland and the Vienna basin respectively. Both publications derive azimuthal anisotropy of Rayleigh waves from ambient-noise correlations at periods that are sensitive to crustal structure. They discuss fast-velocity directions with respect to regional structure and stress field rather than the strength of anisotropy. However, both publications document strong variations in direction of fast velocity with depth (or period), suggesting a weak contribution of the crust to total azimuthal anisotropy in the studied regions. As most studies suggest that the mantle is isotropic below 400-600 km (see review in Savage, 1999 and references therein), SWS is considered as a proxy of strain in the upper mantle.

The numerous observations of SWS from core phases in the greater Alpine region are shown in Fig. 2.7. Most fast polarization directions (FPD) tend to be parallel to the trend of the belt while anisotropy is stronger in the external than in the internal parts of the belt (e.g. Barruol et al. 2004; Barruol et al. 2011; Bokelmann et al. 2013; Qorbani et al. 2015; Salimbeni et al. 2018). These observations have led Barruol et al. (2004, 2011) to propose an asthenospheric source of anisotropy in the western Alps, where present-day or recent mantle flow induced by the retreat of the Apenninic slab would be deflected by the European slab. This hypothesis has been taken up and extended by Salimbeni et al. (2018) who provided additional measurements in the western Alps and the Po plain. Their new observations contradict the proposal by Vignaroli et al. (2008) of a counterclockwise toroidal

flow across the gap between the Alpine and Apenninic slabs. They rather propose that fossil fabrics may be still preserved within the Alpine and Apenninic slabs to explain the weak SWS delay times and the null anisotropy measurements in the Po plain. In the external western Alps, Salimbeni et al. (2018) follow Barruol et al. (2004) in their proposal that arc-parallel fast polarization directions are induced by a suction effect at the scale of the supraslab mantle in response to the progressive rollback of the Apenninic slab. The absence of a counterclockwise toroidal flow at the northern edge of the Apenninic slab could enhance the suction effect in the mantle of the Western Alps.

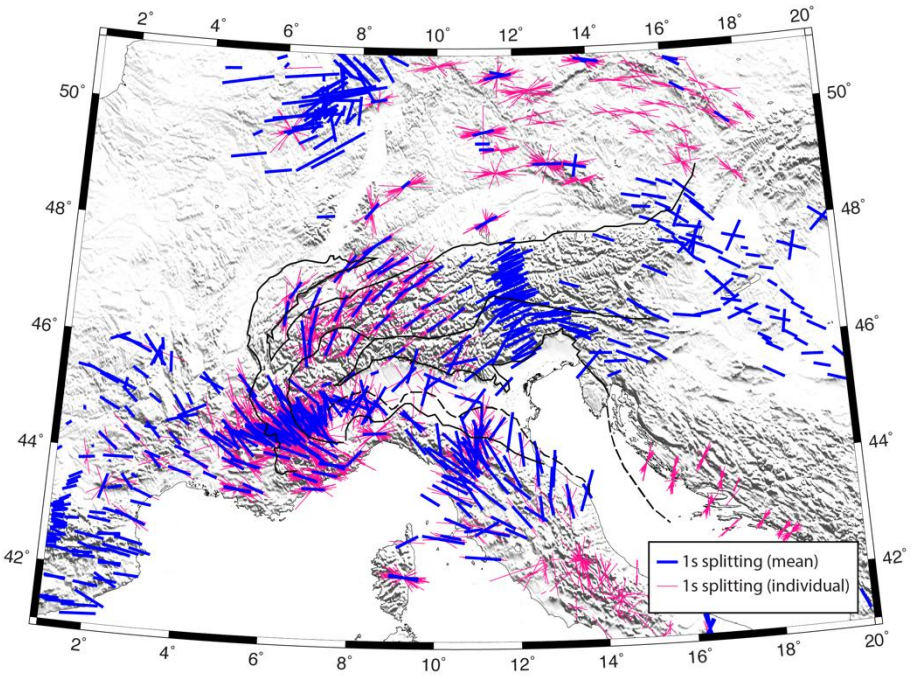

Figure 2.7. *Map of shear-wave splitting measurements in and around the Alps. Station-averaged measurements are shown as thick blue vectors, while individual measurements (from a single earthquake) are shown as thin pink vectors. Vector orientation indicates the fast-polarization (or fast-velocity) direction. Its length is proportional to the time delay between the fast and the slow split phases. Data extracted from the SplitLab SWS database (Barruol et al. 2009; Wüstefeld et al. 2009) complemented with data from Salimbeni et al. (2018).*

In the central and eastern Alps, Bokelmann et al. (2013) and Qorbani et al. (2015) observed a similar simple pattern but with a 45° abrupt change at longitude ~12°E from SW-NE azimuths of the FPD in the west to NW-SE azimuths in the east. This change spatially coincides with the change in the dip of the fast-velocity slab in the upper mantle discussed in section 2.2.1.3, from southward west of 12°E, to vertical-northeastward east of 12°E. To explain the dependence of the splitting parameters with the backazimuth of the incident wave, Qorbani et al. (2015) proposed a two-layer source of anisotropy east of the transition zone. The deeper layer would have a similar FPD as the central Alps (NE-SW), in relation with the eastward-to-vertically dipping high-velocity body interpreted as a detached European slab, while asthenospheric flow above the detached slab would explain the NW–SE FPD of the upper layer.

The quasi-vertical incidence angle of core phases (SKS, SKKS) used in SWS measurements hinders their ability to provide compelling information on the depth of the source of anisotropy. In a recent paper, Löberich and Bokelmann (2020) apply to the central Alps a new procedure based on the use of non-vertical SKS arrivals. Their detailed analysis of SWS observations in the northern central Alps supports with quantitative arguments the hypothesis proposed by Barruol et al. (2011) that the source of the arc-parallel fast polarization directions is asthenospheric flow around the Alpine keels. The characteristics of SWS measurements in the south-central Alps are more complicated and may contain effects of frozen anisotropy in the subduction slabs, as proposed by Salimbeni et al. (2018).

Last but not least, three-dimensional images of azimuthal (and radial) anisotropy beneath the Alps have been computed by Zhu et al. (2015) using FWI of regional earthquake records (including both long-period surface waves and short-period body waves) on a European scale, and by Hua et al. (2017) using joint inversions of arrival time data of local earthquakes and teleseismic events on the Alpine belt. As mentioned above for isotropic velocity, the azimuthal anisotropy model of Zhu et al. (2015) has a low resolution and shows a large-scale variation of fast-velocity directions (FVD) from NW-SE in the western Alps to N-S in the eastern Alps at depths of 100 km to 200 km. The spatial resolution is better in the model of Hua et al. (2017) that displays a similar arc-parallel trend of FVD as the shear-wave splitting measurements. The difference in anisotropy amplitude between the outer and the inner parts of the range is however much less clear in their model than in the SWS results of Fig. 2.7. The greatest variation in anisotropic parameters with depth is observed around 100 km, and these parameters vary little in the upper mantle. Consequently, the 3-D model of Hua et al. (2017) does not provide convincing evidence on the source of azimuthal anisotropy. The origin of this problem is

perhaps to be found in the assumption of horizontal azimuthal anisotropy, which is wrong in strongly dipping subduction slabs.

2.3. Conclusion

Compared to the Himalaya-Tibet system or the Andes, the Alps are a small mountain range. Yet they have a special place in all textbooks on continental collision because the amount of geological data available is unmatched for any other orogen, to paraphrase Kissling (1993) but replacing “geophysical” by “geological”. Since the early 2000s, several geophysical experiments have been conducted in an attempt to bridge the huge gap between the level of geological and geophysical knowledge. Indeed, the Alps, as part of the intricate subduction-collision system of the Mediterranean region, have a complex structure that is difficult to probe. New imaging methods, such as ambient noise tomography or full waveform inversion, have improved the resolution and reliability of images of the crust and upper mantle. New seismic experiments with close station spacing have brought the resolution of tomography closer to the scale of geological observations, but such experiments are generally confined to a profile and tomography is limited to a 2-D section. In combination with permanent networks, the AlpArray seismic experiment (2016-2020) has provided uniform coverage of the greater Alpine region and an unprecedented wealth of data for one of the most emblematic collision belts. The analysis of this unique data set has just started and it will continue for several years ahead. For studies of the crust and mantle structure of the Alps, the data revolution has only just begun.

Acknowledgements

This chapter was written while I was P.I. of the AlpArray-FR project, the French component of the AlpArray initiative, which was funded by Agence Nationale de la Recherche (contract ANR-15-CE31-0015) and Labex OSUG@2020 (Investissement d’Avenir, ANR-10-LABX-56). The CIFALPS project, which was also key in my recent work on the western Alps is supported by the China Academy of Sciences (CAS) and the National Natural Science Foundation of China (NSFC). I warmly thank my colleagues of the CIFALPS team who made it possible for our field and research work on the western Alps to be carried out in such a pleasant and stimulating atmosphere. I also thank E. Kästle for his useful plots that compare the results of the numerous tomographies of the Alpine mantle. Reviews by G. Bokelmann and an anonymous reviewer were of great help to improve this chapter.

References

Aki, K., Christoffersson, A., Husebye, E. S. (1976). Three-dimensional seismic structure of the lithosphere under Montana Lasa, Bull. Seis. Soc. Am., 66 (2): 501–524.

AlpArray Seismic Network (2014). Eastern Alpine Seismic Investigation (EASI) - AlpArray Complimentary Experiment. AlpArray Working Group. doi: 10.12686/alparray/xt_2014.

AlpArray Seismic Network (2015), AlpArray Seismic Network (AASN) temporary component. AlpArray Working Group. Other/Seismic Network, doi:10.12686/alparray/z3_2015

Babuška, V., Plomerova, J., Granet, M. (1990), The deep lithosphere in the Alps: a model inferred from P residuals, Tectonophysics, 176, 137-165.

Barruol, G., Deschamps, A., Coutant, O. (2004). Mapping upper mantle anisotropy beneath SE France by SKS splitting indicates Neogene asthenospheric flow induced by Apenninic slab roll-back and deflected by the deep Alpine roots, Tectonophysics, 394, 125-138.

Barruol, G., Wüstefeld, A., Bokelmann, G. (2009). SKS-splitting-database. Université de Montpellier, Laboratoire Géosciences, doi:10.18715/sks_splitting_database

Barruol, G., Bonnin, M., Pedersen, H., Bokelmann, G.H.R., Tiberi, C. (2011). Belt-parallel mantle flow beneath a halted continental collision: The Western Alps, Earth and Planetary Science Letters, 302, 429-438.

Bayer, R., Carozzo, M.T., Lanza, R., Miletto, M., Rey, D. (1989). Gravity modelling along the ECORS-CROP vertical seismic profile through the Western Alps, Tectonophysics, 162, 203-218.

Behm, M., Brueckl, E., Chwatal, W., Thybo, H. (2007). Application of stacking and inversion techniques to three-dimensional wide-angle reflection and refraction seismic data of the Eastern Alps, Geophys. J. Int., 170, 275–298.

Beller S., Monteiller, V., Operto, S., Nolet, G., Paul, A., Zhao L. (2018). Lithospheric architecture of the South-Western Alps revealed by multi-parameter teleseismic full-waveform inversion, Geophys. J. Int., 212, 1369–1388.

Bokelmann, G., Qorbani, E., Bianchi, I. (2013). Seismic anisotropy and large-scale deformation of the Eastern Alps, Earth and Planetary Science Letters 383, 1–6.

Bonvalot, S., Balmino, G., Briais, A., Kuhn, M., Peyrefitte, A., Vales, N. et al. (2012). World Gravity Map. Bureau Gravimetrique International (BGI), map, CGMW-BGI-CNES-IRD Ed., Paris.

Blundell, D., Freeman, R., Mueller, S., Button, S. (eds) (1992). A continent revealed - The European Geotraverse, Cambridge University Press, 275 pp.

Campillo, M., Paul, A. (2003). Long range correlations in the diffuse seismic coda, Science, 299, 547-549.

Cattaneo, M., Eva, C. (1990). Propagation anomalies in Northwestern Italy by inversion of teleseismic residuals, Terra Nova, 2, 577-584.

Chopin, C. (1984). Coesite and pure pyrope in high-grade blueschists of the Western Alps: A first record and some consequences, Contributions to Mineralogy and Petrology, 86, 107–118.

Closs, H., Labrouste, Y. (1963). Recherches séismologiques dans les Alpes Occidentales au moyen des grandes explosions en 1956, 1958 et 1960, in : Année Géophysique Internationale, XII, 2: CNRS, Paris, 241 pp.

Diehl, T., Husen, S., Kissling, E., Deichmann, N. (2009). High-resolution 3-D P-wave model of the Alpine crust, Geophys. J. Int., 179, 1133–1147.

Di Stefano, R., Kissling, E., Chiarabba, C., Amato, A., Giardini, D. (2009). Shallow subduction beneath Italy: Three-dimensional images of the Adriatic-European-Tyrrhenian lithosphere system based on high-quality P wave arrival times, J. Geophys. Res., 114, B05305.

Dumont T., Schwartz, S., Guillot, S., Simon-Labric, T., Tricart, P., Jourdan, S. (2012). Structural and sedimentary records of the Oligocene revolution in the Western Alpine arc, Journal of Geodynamics, 56–57, 18–38.

Fichtner, A., van Herwaarden, D.-P., Afanasiev, M., Simutè, S., Krischer, L., Çubuk-Sabuncu, Y. et al. (2018). The Collaborative Seismic Earth Model: Generation 1. Geophysical Research Letters, 45, 4007–4016.

Fox, M., Herman, F., Kissling, E., Willett, S. D. (2015). Rapid exhumation in the Western Alps driven by slab detachment and glacial erosion, Geology, 43 (5), 379–382.

Frei, W., Heitzmann, P., Lehner, P. (1990). Swiss NFP-20 research program of the deep structure of the Alps, Mém. Soc. Géol. Fr., 156, 29-46.

Fry, B., Deschamps, F., Kissling, E., Stehly, L., Giardini, D. (2010). Layered azimuthal anisotropy of Rayleigh wave phase velocities in the European Alpine lithosphere inferred from ambient noise, Earth Planet. Sci. Lett. 297, 95-102.

Giacomuzzi, G., Chiarabba, C., De Gori, P. (2011). Linking the Alps and Apennines subduction systems: New constraints revealed by high-resolution teleseismic tomography, Earth and Planetary Science Letters 301, 531–543.

Guillot, S., Hattori, K., Agard, P., Schwartz, S., Vidal, O. (2009). Exhumation processes in oceanic and continental subduction contexts: A review, in Subduction Zone Geodynamics, S. Lallemand & F. Funiciello (eds), pp. 175-205, Springer-Verlag Berlin Heidelberg.

Heit, B., Weber, M., Haberland, C., Tilmann, F., Hemmleb, S, Schwarz, S., Handy, M., Jia, Y., Pesaresi, D. (2018). The AlpArray SWATH-D experiment. Geophysical Research Abstracts Vol. 20, EGU2018-11509, 2018 EGU General Assembly.

Heit, B., Weber, M., Tilmann, F., Haberland, C., Jia, Y., Carraro, C., Walcher, G., Franceschini, A., Pesaresi, D. (2017). The Swath-D Seismic Network in Italy and Austria. GFZ Data Services. doi: 10.14470/MF7562601148

Hetényi, G., Molinari, I., Clinton, J. et al. (2018a). The AlpArray Seismic Network: A large-scale European experiment to image the Alpine orogeny, Surv. Geophys., 39, 1009–1033.

Hetényi, G., Plomerová, J., Bianchi, I., Exnerová, H. K., Bokelmann, G., Handy, M. R., Babuška, V., AlpArray-EASI Working Group (2018b). From mountain summits to roots: Crustal structure of the Eastern Alps and Bohemian Massif along longitude 13.3°E, 744, 239-255, Tectonophysics 744, 239-255.

Hua, Y., Zhao, D., Xu, Y. (2017). P wave anisotropic tomography of the Alps, J. Geophys. Res. Solid Earth, 122, 4509–4528.

Jolivet, L., Faccenna, C. (2000). Mediterranean extension and the Africa-Eurasia collision, Tectonics, 19, 1095-1106.

Kästle, E. D., El-Sharkawy, A., Boschi, L., Meier, T., Rosenberg, C., Bellahsen, N., Cristiano, L., Weidle, C. (2018). Surface wave tomography of the Alps using ambient-noise and earthquake phase velocity measurements, J. Geophy. Res.: Solid Earth, 123, 1770–1792.

Kästle E. D., Rosenberg, C., Boschi, L., Bellahsen, N., Meier, T., El-Sharkawy, A. (2020). Slab break-offs in the Alpine subduction zone, International Journal of Earth Sciences, 109, 587–603.

Kissling, E. (1993). Deep structure of the Alps – what do we really know? Physics of the Earth and Planetary Interiors, 79, 87-112.

Koulakov, I., Kaban, M. K., Tesauro, M., Cloetingh, S. (2009). P- and S-velocity anomalies in the upper mantle beneath Europe from tomographic inversion of ISC data, Geophys. J. Int., 179, 345–366.

Kummerow, J., Kind, R., Oncken, O., Giese, P., Ryberg, T., Wylegalla, K., Scherbaum, F., TRANSALP Working Group (2004). A natural and controlled source seismic profile through the Eastern Alps: TRANSALP, Earth and Planetary Science Letters, 225, 115–129.

Lardeaux, J.M., Schwartz, S., Tricart, P., Paul, A., Guillot, S., Béthoux, N., Masson, F. (2006). A crustal-scale cross-section of the south-western Alps combining geophysical and geological imagery, Terra Nova, 18, 412–422.

Lippitsch, R., Kissling, E., Ansorge, J. (2003). Upper mantle structure beneath the Alpine orogen from high resolution teleseismic tomography, J. Geophy. Res., 108, B82376.

Löberich, E., Bokelmann, G. (2020). Mantle flow under the Central Alps: Constraints from non-vertical SKS shear-wave splitting, Solid Earth Discussions [preprint], 1-4.

Lombardi, D., Braunmiller, J., Kissling, E., Giardini, D. (2008). Moho depth and Poisson's ratio in the Western–Central Alps from receiver functions, Geophys. J. Int., 173, 249–264.

Lu, Y., Stehly, L., Paul, A., AlpArray Working Group (2018). High-resolution surface wave tomography of the European crust and uppermost mantle from ambient seismic noise, Geophys. J. Int., 214,1136-1150.

Lu, Y., Stehly, L., Brossier, R., Paul, A., AlpArray working group (2020). Imaging Alpine crust using ambient noise wave-equation tomography, Geophys. J. Int., 222, 69-85.

Lüschen E., Borrini, D., Gebrande, H., Lammerer, B., Millahn, K., Neubauer, F., Nicolich, R., TRANSALP Working Group (2006). TRANSALP—deep crustal Vibroseis and explosive seismic profiling in the Eastern Alps, Tectonophysics 414, 9–38.

Lyu, C., Pedersen, H. A., Paul, A., Zhao, L., Solarino, S., CIFALPS Working Group (2017). Shear wave velocities in the upper mantle of the Western Alps: new constraints using array analysis of seismic surface waves, Geophys. J. Int., 210, 321–331.

Maffione, M., Speranza, F., Faccenna, C., Cascella, A., Vignaroli, G., Sagnotti, L. (2008). A synchronous Alpine and Corsica-Sardinia rotation, J. Geophys. Res. Solid Earth, 113, B03104.

Malusà, M. G., Faccenna, C., Baldwin, S. L., Fitzgerald, P. G., Rossetti, F., Balestrieri, M. L., Danisik, M., Ellero, A., Ottria, G., Piromallo, C. (2015). Contrasting styles of (U)HP rock exhumation along the Cenozoic Adria-Europe plate boundary (Western Alps, Calabria, Corsica), Geochem. Geophys. Geosyst., 16.

Malusà, M. G., Anfinson, O. A., Dafov, L. N., Stockli D. F. (2016). Tracking Adria indentation beneath the Alps by detrital zircon U-Pb geochronology: Implications for the Oligocene–Miocene dynamics of the Adriatic microplate, Geology, 44(2), 155–158.

Mitterbauer, U., Behm, M., Brückl, E., Lippitsch, R., Guterch, A., Keller, G. R., Koslovskaya, E., Rumpfhuber, E-M., Šumanovac, F. (2011). Shape and origin of the East-Alpine slab constrained by the ALPASS teleseismic model, Tectonophysics, 510, 195–206.

Molinari, I., Verbeke, J., Boschi, L., Kissling, E., Morelli, A. (2015a). Italian and Alpine three-dimensional crustal structure imaged by ambient-noise surface-wave dispersion, Geochem. Geophys. Geosyst., 16.

Molinari, I., Argnani, A., Morelli, A., Basini, P. (2015b). Development and testing of a 3-D seismic velocity model of the Po plain sedimentary basin, Italy, Bull. Seism. Soc. Am., 105, 753–764.

Molinari, I., Morelli, A. (2011). EPcrust: a reference crustal model for the European Plate, Geophys. J. Int., 185, 352–364.

Nicolas, A., Christensen, N. I. (1987). Formation of anisotropy in upper mantle peridotites- A review, in: Composition, Structure and Dynamics of the Lithosphere-Asthenosphere System, Vol. 16 (Fuchs, K. & Froidevaux, C. eds), pp. 111-123, Am. Geophys. Un., Washington D.C.

Nicolas, A., Hirn, A., Nicolich, R., Polino, R., ECORS-CROP Working Group (1990). Lithospheric wedging in the western Alps inferred from the ECORS-CROP traverse, Geology, 18, 587–590.

Nocquet, J.-M., Sue, C., Walpersdorf, A., Tran, T., Lenôtre, N., Vernant, P., Cushing, M., Jouanne, F., Masson, F, Baize, S, Chéry, J., van der Beek, P. A. (2016). Present-day uplift of the western Alps, Scientific Reports 6, 28404.

Paffrath, M., Friederich, W., AlpArray Working Group (2020). Teleseismic P-wave travel time tomography of the Alpine upper mantle using AlpArray seismic network data, EGU2020-13779, EGU General Assembly 2020.

Paul, A., Cattaneo, M., Thouvenot, F., Spallarossa, D., Béthoux, N., Fréchet, J. (2001). A three-dimensional crustal velocity model of the south-western Alps from local earthquake tomography, J. Geophys. Res., 106, 19367-19389.

Piana Agostinetti, N., Amato, A. (2009). Moho depth and Vp/Vs ratio in peninsular Italy from teleseismic receiver functions, J. Geophys. Res., 114, B06303.

Piromallo, C., Morelli, A. (2003). P wave tomography of the mantle under the Alpine-Mediterranean area, J. Geophys. Res., 108, B22065.

Piromallo, C., Faccenna, C. (2004). How deep can we find the traces of Alpine subduction? Geophys. Res. Lett., 31, L06605.

Potin B. (2016). Les Alpes occidentales : tomographie, localisation de séismes et topographie du Moho, Ph-D thesis, Université Grenoble Alpes.

Qorbani E., Bianchi, I., Bokelmann, G. (2015). Slab detachment under the Eastern Alps seen by seismic anisotropy, Earth and Planetary Science Letters 409, 96–108.

Reynard, B. (2013). Serpentine in active subduction zones, Lithos, 178, 171-185

Salimbeni S., Malusà, M.G., Zhao, L., Guillot, S., Pondrelli, S., Margheriti, L., Paul, A., Solarino, S., Aubert, C., Dumont, T., Schwartz, S., Wang, Q., Xu, X., Zheng, T., Zhu, R. (2018). Active and fossil mantle flows in the western Alpine region unravelled by seismic anisotropy analysis and high-resolution P wave tomography, Tectonophysics, 731, 35-47.

Savage, M. (1999). Seismic anisotropy and mantle deformation: What have we learned from shear wave splitting? Rev. Geophys., 37, 65–106.

Schippkus, S., Zigone, D., Bokelmann, G., AlpArray Working Group (2020). Azimuthal anisotropy in the wider Vienna basin region: a proxy for the present-day stress field and deformation, Geophys. J. Int., 220, 2056-2067.

Shapiro, N.M., Campillo, M. (2004). Emergence of broadband Rayleigh waves from correlations of the ambient seismic noise, Geophys. Res. Lett., 31, L07614.

Shapiro, N. M., Campillo, M., Stehly, L., Ritzwoller, M. H. (2005). High-resolution surface-wave tomography from ambient seismic noise, Science, 307, 1615-1618.

Silver, P. G., Chan, W. W. (1991). Shear wave splitting and subcontinental mantle deformation, J. Geophys. Res., 96, B10, 16429-16454.

Solarino S., Malusà, M.G., Eva, E., Guillot, S., Paul, A., Zhao, L., Aubert, C., Dumont, T., Pondrelli, S., Salimbeni, S., Schwartz, S., Wang, Q., Xu, X., Zheng, T., Zhu, R. (2018). Mantle wedge exhumation beneath the Dora-Maira (U)HP dome unravelled by local earthquake tomography (Western Alps), Lithos, 296-299, 623-636.

Spada, M., Bianchi, I., Kissling, E., Piana Agostinetti, N., Wiemer, S. (2013). Combining controlled-source seismology and receiver function information to derive 3-D Moho topography for Italy, Geophys. J. Int., 194, 1050–1068.

Spakman, W. (1990). Tomographic images of the upper mantle below central Europe and the Mediterranean, Terra Nova, 2, 542-553.

Spakman, W. (1991). Delay-time tomography of the upper mantle below Europe, the Mediterranean, and Asia Minor, Geophys. J. Int., 107, 309-332.

Stehly, L., Fry, B., Campillo, M., Shapiro, N.M., Guilbert, J., Boschi, L., Giardini, D. (2009). Tomography of the Alpine region from observations of seismic ambient noise, Geophys. J. Int., 178, 338–35.

Sternai, P., Sue, C, Husson, L., Serpelloni, E., Becker, T. W., Willett, S. D., Faccenna, C., Di Giulio, A., Spada, G., Jolivet, L., Valla, P., Petit, C., Nocquet, J-M., Walpersdorf, A., Castelltort, S. (2019). Present-day uplift of the European Alps: Evaluating mechanisms and models of their relative contributions, Earth-Science Reviews 190, 589–604.

Tape C., Liu, Q., Maggi, A., Tromp, J. (2009). Adjoint tomography of the Southern California crust, Science, 325, 988-992.

Thouvenot, F., Paul, A., Fréchet, J., Béthoux, N., Jenatton, L., Guiguet, R. (2007). Are there superposed Mohos in the south-western Alps? New seismic data from fan-profiling reflections, Geophys. J. Int., 170, 1180–1194.

Thurber, C.H. (1983). Earthquake locations and three-dimensional crustal structure in the Coyote Lake area, central California, J. Geophys. Res., 88, 8226-8236.

Vignaroli, G., Faccenna, C., Jolivet, L., Piromallo, C., Rossetti, F. (2008). Subduction polarity reversal at the junction between the Western Alps and the Northern Apennines, Italy, Tectonophysics 450 (2008) 34–50.

Vinnik, L.P. (1977). Detection of waves converted from P to SV in the mantle, Phys. Earth Planet. Int., 15, 39-45.

Wagner, M., Kissling, E., Husen, S. (2012). Combining controlled-source seismology and local earthquake tomography to derive a 3-D crustal model of the western Alpine region, Geophys. J. Int. 191, 789–802.

Waldhauser F., Kissling, E., Ansorge, J., Mueller, S. (1998). Three-dimensional interface modelling with two-dimensional seismic data: The Alpine crust–mantle boundary, Geophys. J. Int. 135, 264–278.

Waldhauser, F., Lippitsch, R., Kissling, E., Ansorge, J. (2002). High-resolution teleseismic tomography of upper-mantle structure using an *a priori* three-dimensional crustal model, Geophys. J. Int. (2002) 150, 403–414

Wüstefeld, A., Bokelmann, G. H. R., Barruol, G., Montagner, J.-P. (2009). Identifying global seismic anisotropy patterns by correlating shear-wave splitting and surface waves data, Phys. Earth Planet. Int., 176 (3-4), 198-212.

Zahorec, P., Papčo, J., Pašteka, R., Bielik, M., Bonvalot, S., Braitenberg, C., Ebbing, J., Gabriel, G., Gosar, A., Grand, A., Götze, H.-J., Hetényi, G., Holzrichter, N., Kissling, E., Marti, U., Meurers, B., Mrlina, J., Nogová, E., Pastorutti, A., Scarponi, M., Sebera, J., Seoane, L., Skiba, P., Szűcs, E., and Varga, M. (2021). The first pan-Alpine surface-gravity database, a modern compilation that crosses frontiers, Earth Syst. Sci. Data, 13, 2165-2209.

Zhao, L., Paul, A., Guillot, S., Solarino, S., Malusà, M. G., Zheng, T., Aubert, C., Salimbeni, S., Dumont, T., Schwartz, S., Zhu, R., Wang, Q. (2015). First seismic evidence for continental subduction beneath the Western Alps, Geology, 43, 9, 815-818.

Zhao, L., Paul, A., Solarino, S., RESIF (2016a). Seismic network YP: CIFALPS temporary experiment (China–Italy–France Alps seismic transect), RESIF - Réseau Sismologique et géodésique Français, doi:10.15778/RESIF.YP2012.

Zhao, L., Paul, A., Malusà, M. G, Xu, X., Zheng, T., Solarino, S., Guillot, S., Schwartz, S., Dumont, T., Salimbeni, S., Aubert, C., Pondrelli, S., Wang, Q., Zhu, R. (2016b). Continuity of the Alpine slab unraveled by high-resolution P-wave tomography, J. Geophys. Res. Solid Earth, 121, 8720-8737.

Zhao, L., Malusà, M. G, Yuan, H., Paul, A., Guillot, S., Lu, Y., Stehly, L., Solarino, S., Eva, E., Lu, G., Bodin, T., Cifalps group, AlpArray Working Group (2020). Evidence for a serpentinized plate interface favouring continental subduction, Nature Communications, 11, 2171.

Dueker, K. G., Sheehan, A. F. (1997). Mantle discontinuity structure from midpoint stacks of converted P to S waves across the Yellowstone hotspot track. Journal of Geophysical Research, 102, 8313–8327.

Zhu, H., Bozdag, E., Tromp, J. (2015). Seismic structure of the European upper mantle based on adjoint tomography, Geophys. J. Int., 201, 18–52.